Appl. Math. Mech. -Engl. Ed., **33**(12), 1481–1492 (2012)
DOI 10.1007/s10483-012-1638-x

Applied Mathematics and Mechanics (English Edition)

Properties of acoustic resonance in double-actuator ultra-sonic gas nozzle: numerical study*

Hong-biao ZU (祖洪彪)[1,2,3], Zhe-wei ZHOU (周哲玮)[1,2,3], Zhi-liang WANG (王志亮)[1,2,3]

(1. Shanghai Institute of Applied Mathematics and Mechanics, Shanghai University, Shanghai 200072, P. R. China;
2. Shanghai Key Laboratory of Mechanics in Energy Engineering, Shanghai University, Shanghai 200072, P. R. China;
3. Modern Mechanics Division, E-Institutes of Shanghai Universities, Shanghai University, Shanghai 200072, P. R. China)

Abstract The ultra-sonic gas atomization (USGA) nozzle is an important apparatus in the metal liquid air-blast atomization process. It can generate oscillating supersonic gas efflux, which is proved to be effective to enforce the atomization and produce narrow-band particle distributions. A double-actuator ultra-sonic gas nozzle is proposed in the present paper by joining up two active signals at the ends of the resonance tubes. Numerical simulations are adopted to study the effects of the flow development on the acoustic resonant properties inside the Hartmann resonance cavity with/without actuators. Comparisons show that the strength and the onset process of oscillation are enhanced remarkably with the actuators. The multiple oscillating amplitude peaks are found on the response curves, and two kinds of typical behaviors, i.e., the Hartmann mode and the global mode, are discussed for the corresponding frequencies. The results for two driving actuators are also investigated. When the amplitudes, the frequencies, or the phase difference of the input signals of the actuators are changed, the oscillating amplitudes of gas efflux can be altered effectively.

Key words spray atomization, ultra-sonic gas nozzle, resonance, numerical simulation

Chinese Library Classification O327
2010 Mathematics Subject Classification 74D05

1 Introduction

Hartmann and Trolle[1] found the resonance phenomena of a tube in the experiment in 1919. Then, many theoretical and experimental studies were carried out to investigate the mechanism[2]. Grant[3] invented an ultra-sonic gas atomization (USGA) nozzle in spray atomization by the effects of the Hartmann resonance tube. In spray forming technology, spray

* Received Feb. 14, 2011 / Revised Sept. 21, 2012
Project supported by the National Natural Science Foundation of China (Nos. 10772107, 10702038, and 11172163), the E-Institutes of Shanghai Municipal Education Commission, and the Shanghai Program for Innovative Research Team in Universities
Corresponding author Zhi-liang WANG, Ph. D., E-mail: wng_zh@shu.edu.cn

atomization is formed mainly using the high-speed gas flow to fragmentize the molten metal jet into small fractals. The nozzle is an important part of a spray atomizer. There are two kinds of atomizing nozzles in use generally, the USGA nozzle presented by Grant[3] and the high-pressure gas atomization (HPGA) nozzle presented by Ayres and Anderson[4]. At present, the HPGA nozzle is widely used in the industrial applications, and the related research is also very active[5–7].

The sizes and the distribution of atomized metal droplets can affect the quality of products. Experiments indicate that the small average size and the relative narrow-band distribution of droplets, which are helpful to improve the quality of spray injection products[3,8], can be produced when oscillations are introduced into the gas atomization. The secondary resonance tube formation in the USGA nozzle can help generate high frequency oscillations in the outlet flow even though the upstream flow is steady[9]. Zhou and Tang[10] indicated that the parametric resonance between the oscillating gas flow and the liquid metal flow is probably the reason of this improvement.

Veistinen et al.[11] proposed a "self-adjusting throat" hypothesis to explain how the gas flow was accelerated from subsonic to supersonic in the nozzle. Mansour et al.[12] simulated the steady flow structure inside the USGA nozzle. Li et al.[9] investigated the USGA nozzle numerically by the finite volume method based on the Roe solver. They studied the effects of variation of parameters on the oscillation and discussed the mechanism of transition from subsonic to supersonic.

Wang[13] proposed a positive actuator into the USGA nozzle to enhance the resonance and control the efflux properties. Zu and Wang[14] tested it numerically and verified that the actuator can effectively influence and enhance the mass flow rate and the pressure oscillating amplitude at the nozzle outlet. In a certain range of the driving frequency and the strength, several resonance frequencies were found.

In the present paper, the work of Wang[13] and Zu and Wang[14] is extended, and a new double-actuator USGA nozzle is proposed (see Fig. 1). A main actuator and an auxiliary actuator are introduced into the prototype of the USGA nozzle. The characteristics of the interior flow and the outlet flow are studied numerically.

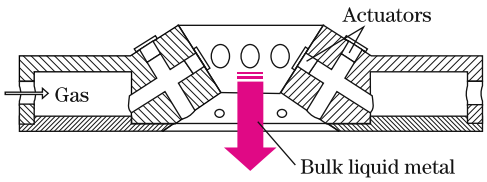

Fig. 1 Diagram of nozzle in double-actuator USGA

2 Physical and numerical models

The double-actuator USGA nozzle is so complex that it makes the direct numerical study unrealistic. We create a simplified USGA nozzle model including the inflow and outflow ducts and the resonance region (see Fig. 2(a)). The sketch of the computational region and the meshes are shown in Fig. 2. The resonance tube length and the secondary resonance tube length are represented by L_1 and L_2. The lengths of the inflow and outflow ducts are represented by L_3 and L_4. The diameter of the tube is $D = 3.6$ mm. The actuators are placed at the ends of the tubes.

The boundary conditions are important in the numerical simulations. Here, we set the pressure of the outlet to be P_{out} and the pressure of the inlet to be P_{in}. Thus, we obtain the outlet/inlet pressure ratio $R = P_{\text{out}}/P_{\text{in}}$. The role of the actuator is to generate controllable oscillation, which is realized by a zero mass-flux jet. A no-slip adiabatic wall boundary condition

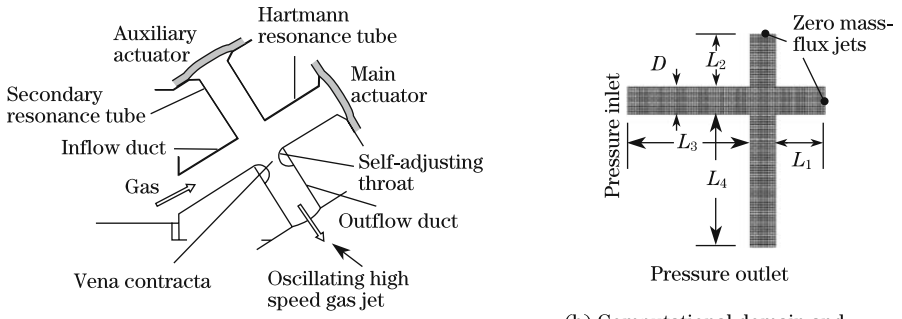

(a) Resonance cavity (not to scale)

(b) Computational domain and boundaries

Fig. 2 Sketch of resonance cavity in double-actuator USGA nozzle and computational domain

is set at the tube wall. A time-dependent mass-flux inlet condition is used as the above-mentioned zero mass-flux jet using the user-defined-function (UDF) module on the FLUENT platform as follows[14]:

$$\Phi_{\mathrm{mass},i} = A_i \sin(2\pi f_i t + \varphi_i), \tag{1}$$

where A, f, and φ correspond to the amplitude, frequency, and phase of the mass influx of the actuator, respectively. Subscript $i = \mathrm{M}$ or S indicates the main actuator or the auxiliary actuator. Note that the parameters in Eq. (1) are dimensional.

3 Verification of computational tools

The transient two-dimensional (2D) simulations are carried out on the FLUENT platform with an implicit segregated solver on the square meshes generated by Gambit. As shown in Fig. 3, different turbulence models are adopted to testify the validation of numerical results. It shows that the pressure oscillation of the laminar model is greater than that of the turbulent models, which may owe to the turbulence energy loss that is not considered in the laminar model. Here, we adopt the Spalart-Allmaras turbulence model[15], which is a one-equation model with less time consumption, giving good results for the wall-bounded flow and the boundary layers with adverse pressure gradients. The standard values of the constants ($C_{\mathrm{b1}}=0.135\,5$, $C_{\mathrm{b2}}=0.622$, $C_{\mathrm{w1}}=7.1$, $C_{\mathrm{w2}}=0.3$, $C_{\mathrm{w3}}=2$, $Pr=0.667$, $Pr_{\mathrm{E}}=Pr_{\mathrm{W}}=0.85$, where Pr_{E} is the energy Prandtl number, and Pr_{W} is the wall Prandtl number) are used for turbulence modeling (for the details of these variables, see [14]). The time step is $\Delta t = 10\mathrm{E}{-}06\,\mathrm{s}$.

According to the simulations on the USGA nozzle of $L_1 = L_2$ in the work of Li et al.[9], the frequency of gas oscillation can be correlated with that of the Hartmann whistle under the jet regurgitant mode. Hence, the frequencies for both the USGA nozzle and the Hartmann whistle can be represented by a linear acoustic theoretical formula $\omega = c/4L$[16] (where c is the local speed of the sound, and L is the effective length of the resonance tube[17]). For testing the three-dimensional (3D) effects, we also do the 3D simulations (see Fig. 4) for $D \leqslant L_1 = L_2 \leqslant 4D$, and make comparisons of the frequencies of oscillation with the theoretical curve and datum in [5]. The 3D simulations are executed with the same model and boundary conditions as the 2D simulations except for the different geometrical models on the tetrahedron meshes. The present results are slightly different from those in [9] but with the same trend and show good agreement with the theoretical predictions[16] (see Fig. 5). They all show that the frequency of oscillation decreases when the length of the Hartmann resonance tube increases with $L_1 = L_2$. It shows that the differences of frequencies between the 3D and the 2D simulations are negligible. Here, we take the 2D simulations for the sake of the computation cost.

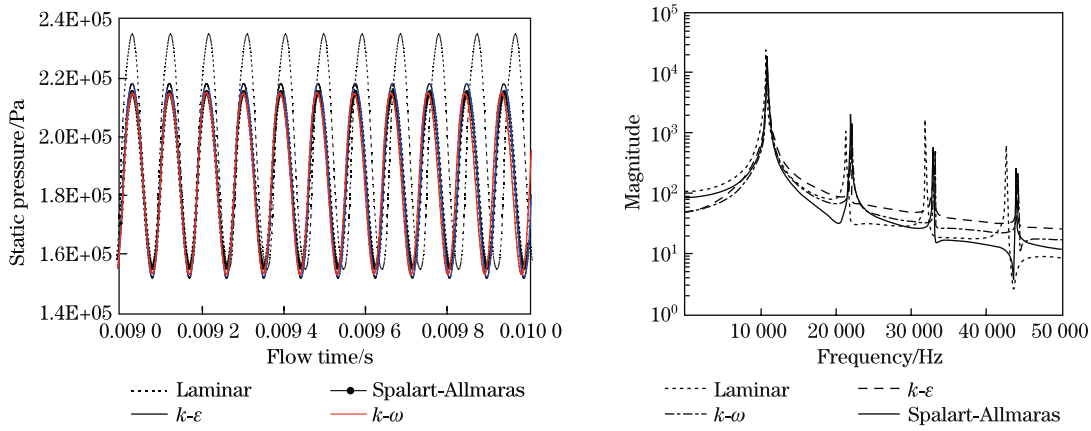

(a) Oscillation of static pressure (b) Spectral analysis of static pressure

Fig. 3 Turbulent model: pressure-time curve (a) and frequency spectrogram (b) at bottom of resonance tube

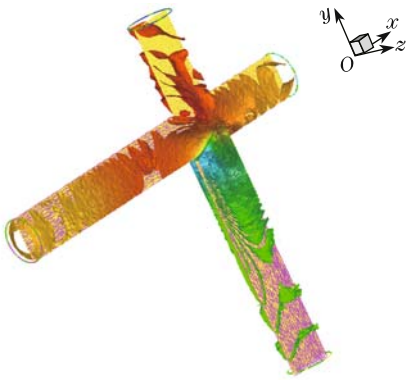

Fig. 4 Calculating chart of 3D isobaric surfaces and centre-sectional velocity vectors of USGA nozzle

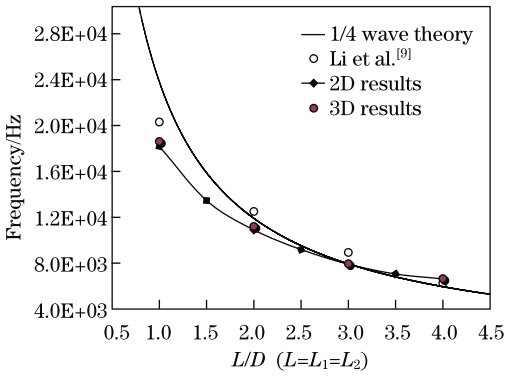

Fig. 5 Comparisons of frequency for USGA nozzle at condition of $L_1 = L_2$

4 Results and discussion

4.1 USGA nozzle resonance characteristics

Besides turning the steady gas flow to oscillate, as the Hartmann whistle does, the USGA nozzle can also accelerate the subsonic intaking gas flow into a supersonic outflow jet. Veistinen et al.[11] proposed a structure named the self-adjusting throat to explain the transmission in the USGA nozzle. It says that the self-adjusting throat, analogous to the Laval nozzle, is a self-motivated convergence-divergence configuration, and the gas flow accelerates from subsonic to supersonic when it passes through its vena contracta. The present data show that the self-adjusting throat is actually not bilateral as it is assumed[11] (see Fig. 2), but rather like a pipe choked by a vortex ring produced in the back-step flow (see Fig. 6). It functions like a Laval nozzle, and accelerates the subsonic gas flow into a supersonic jet (see Fig. 7). In Fig. 7, the interior of the Ma=1 contour line is a supersonic zone, which confirms the conjectures[6–8] for supersonic transition in the USGA nozzle.

Apparently, the shape of the vena contracta is more complex than the two bow-like curves as drawn in Fig. 2. Li et al.[9] computed the flow structure of the velocity field for $L_1 = L_2 = 2D$

at the inlet Mach number Ma=1, and plotted the iso-Mach curve for Ma=1. They also showed the self-adjusting throat and gave the conclusion that the self-adjusting throat has the similar behaviors as the Laval nozzle. Here, we do further observation in detail. Figure 7 gives the iso-Mach curves for Ma=1, $L_1 = L_2 = 2D$, and the outlet/inlet pressure ratio R ranging from 1.600 to 3.000. It is found that R is the dominant parameter for supersonic transition. For $R = 1.600$, the supersonic region enclosed by the $Ma = 1$ curve forms at the location away from the joint corner of back-step. When R increases, the supersonic region (Ma>1) grows gradually, then reaches its maximum between 2 and 3, close to $R = 2.500$, and keeps its shape since $R \geqslant 2.500$.

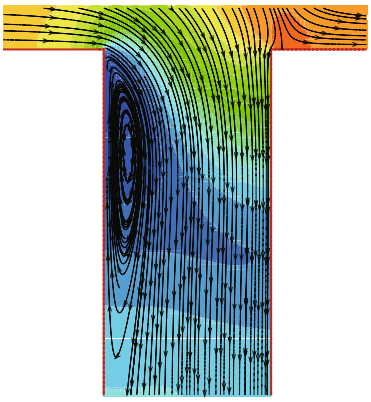

Fig. 6 Streamlines showing back-step flow to form self-adjustable throat

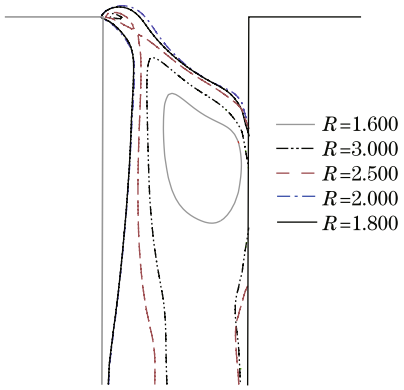

Fig. 7 Contours of $Ma = 1$ for outlet/inlet pressure ratio R from 1.600 to 3.000 at self-adjustable throat

For the case of $L_1 = L_2 = 2D$ and $L_3 = L_4 = 5D$, the situations of the mass flow rate and its fluctuation at the USGA nozzle outlet for $R = 1.050$–3.000 are investigated. The results are shown in Table 1 and Fig. 8. Table 1 shows that the frequency maintains its valve around 10 900 Hz when R increases, and the frequency of fluctuation, a natural frequency of the system, is uncorrelated with R. In contrast, the average mass flow rate increases linearly with R (see Fig. 8). Hence, the maximum mass flow rate limitation for the vena contracta of the Laval nozzle does not happen for the self-adjusting throat of the USGA nozzle. Differently, the amplitude of the mass flow rate has its own inflection point at about R= 2.000, which means that the higher pressure will suppress the fluctuation of the gas flow.

Table 1 Oscillating amplitude and frequency of mass flow rate for $R = 1.000$–3.000 at USGA nozzle outlet

R	$A/(\mathrm{kg \cdot s^{-1}})$	f/Hz
1.175	0.014	10 721.69
1.200	0.017	10 681.19
1.400	0.032	10 822.43
1.500	0.043	10 841.60
1.600	0.058	10 894.82
1.800	0.082	10 899.89
2.000	0.084	10 966.73
2.500	0.081	10 966.73
3.000	0.073	10 984.77

Hence, we recognize that the increase of R can surely increase the outlet flow rate. However, it has the dual effects on the amplitude of gas oscillation, i.e., the higher pressure will accelerate

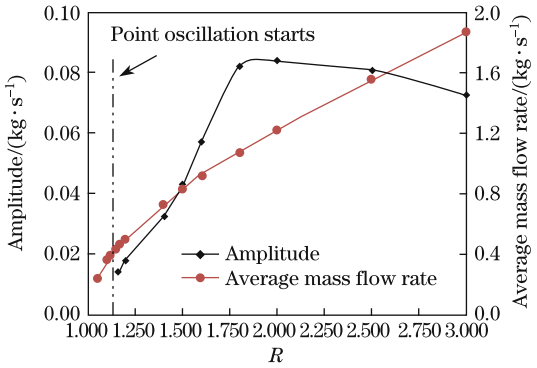

Fig. 8 Curves of average mass flow rate and its oscillating amplitude for $R = 1.000$–3.000 at USGA nozzle outlet

the gas flow, provide more energy, and enhance the oscillation of the gas flow; the sufficiently large pressure will also weaken the compressibility of gas and suppress its oscillating strength.

For the relatively small R, the simulations show that there is a critical value of R for triggering off the gas oscillation. Figure 9 draws two typical curves of the mass flow rate oscillation. When $1.000 < R \leqslant 1.150$, the fluctuation will decay after a transient ripple (see Fig. 9(a)), and for $1.175 \leqslant R \leqslant 3.000$, the fluctuation will grow into a certain amplitude and keep oscillating (see Fig. 9(b)). Obviously, the critical value of R, noted as R_c, of starting oscillation is about 1.150–1.175. Thus, it is not very difficult for a USGA nozzle to start oscillation.

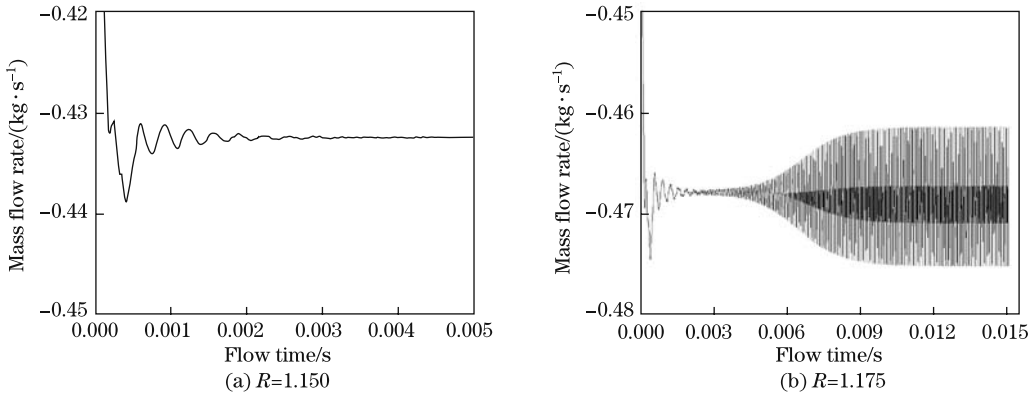

Fig. 9 Curves of mass flow rate near critical outlet/inlet pressure ratio R for starting oscillation

In the practical use, the USGA nozzle has an equal length for the Hartmann resonance tube and the secondary tube, i.e., $L_1 = L_2$. Few literatures involve the vibration property of the inner gas flow for $L_1 \neq L_2$. Here, the numerical experiments are taken to deal with such cases. The related data are shown in Fig. 10, and we connect the points for $L_1 = L_2$ as a reference line. From Fig. 10, it can be find that the natural frequency decreases when L_1 (L_2) increases at the fixed L_2 (L_1) for $L_1 \leqslant L_2$ (the connected lines); while the trend of the fluctuation frequency is not that clear for $L_1 > L_2$ (the points which are not connected by lines). It follows that the influence of the secondary tube should not be overlooked, new theories on the USGA nozzle are necessary to be unveiled, and the theories on the Hartmann whistle may be only correct for

the USGA nozzle at $L_1 = L_2$.

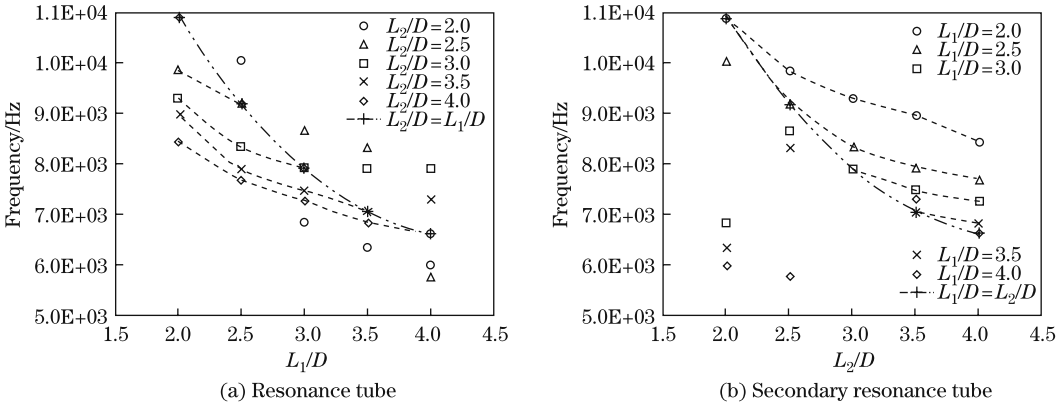

(a) Resonance tube (b) Secondary resonance tube

Fig. 10 Natural frequency for USGA nozzle for different lengths of resonance tube and secondary resonance tube

4.2 Double-actuator USGA nozzle resonance characteristics

To understand the resonance characteristics of a double-actuator USGA nozzle, we focus on the case of $L_1 = L_2 = 2D$, $L_3 = L_4 = 5D$, and $R = 1.600$. The excitation signal is given by Eq. (1).

As a start, the main driving signal is applied to the end of the Hartmann tube[14] with the amplitude of 0.1 kg/s (the inlet mass flow rate is about 1.2 kg/s as a reference), and the phase angle $\varphi = 0$. Increase the excitation frequency f from 0 to 2ω with an increment of 0.05ω, where $f_0 = \omega = 10859$ Hz is the natural frequency of the USGA nozzle without any actuators (the frequency of the Hartmann tube under the Hartmann mode). Correspondingly, the similar manipulation is applied to the secondary tube. Plotting the amplitude curves of the pressure wave and the mass flow rate into the same figure, we have Fig. 11.

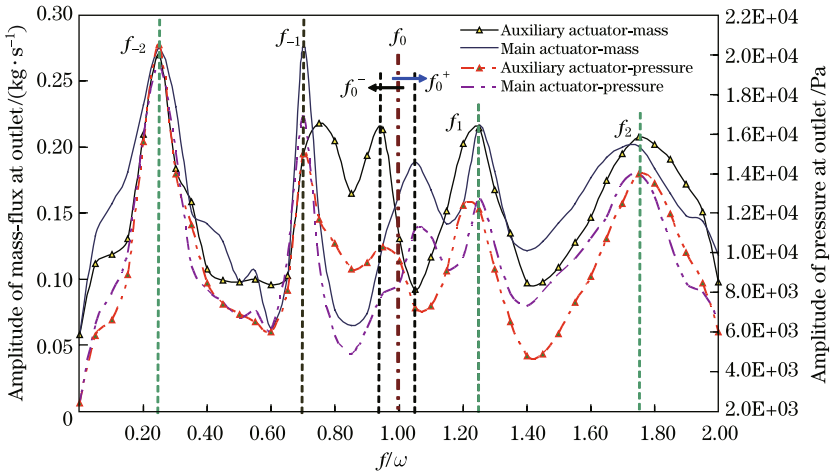

Fig. 11 Amplitudes of fluctuation of mass flow rate and pressure wave at outlet changing with driving frequency when main/auxiliary actuator works independently

Figure 11 clearly shows that the amplitudes of the pressure and the mass flow rate change when the driving frequency increases even under the same excitation intensities. At some certain main driving frequencies, labeled as $f/\omega = 0.25$, 0.70, 1.05, 1.25, and 1.75, the amplitude curves

reach their peaks. Here, the peak value near the natural frequency drifts from $f=1.00\omega$ to $f=f_0^+=1.05\omega$. The amplitude of the outlet mass flow rate is 0.189 kg/s, which exceeds 3 times that of running without an actuator (0.058 kg/s). It shows the possibility of enhancing the vibration strength by actuators. The amplitudes of the pressure and the mass flow rate reach their peak values synchronously. The maximum peak value is also not located at the driving frequency $f=f_0=1.00\omega$ (the natural frequency), and the amplitude is relatively weak when it is compared with other peak values for $f=f_0=1.00\omega$.

The situation seems to be similar to that of an auxiliary actuator. There are also five crests on each curve with the same trends of amplitude variations. Comparing the curves of the auxiliary actuator with those of the main actuator, one can identify that the peak points at $f=f_0=1.00\omega$ are shifted in opposite directions. For the main actuator, the crest locates at $f=f_0^+=1.05\omega$[11] as mentioned above, while for the auxiliary actuator, it locates at $f=f_0^-=0.95\omega$.

The behaviors of the deactuated procedure are also investigated for $f_M/\omega=0.50$, 0.70, 0.95, 1.05, and 1.50. The oscillations of the mass flow rate at the outlet of the USGA nozzle are recorded during the switching processes from applying the main driving signal to deactuating it. The related curves are plotted in Fig. 12.

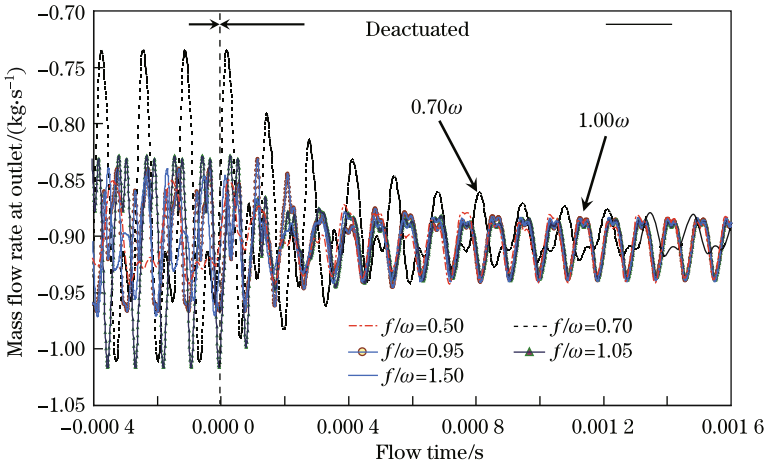

Fig. 12 Deactuated transition curves of fluctuation of mass flow rate with different driving frequencies

Figure 12 shows that all the oscillations finally overlap into two curves with f_M/ω=0.70 and 1.00 after deactuating, which shows that these two frequencies are self-sustainable characteristic frequencies.

Zu and Wang[14] discussed these working modes. They found two basic characteristic frequencies, which correlate with the local geometry and the global geometry of the USGA nozzle, respectively, out of all the excited ones. The local one, namely, the Hartmann mode, is determined by the size of the Hartmann resonance tube. The global one, namely, the global mode, is decided by the structure of cavity. The frequency $f_M=0.70\omega$ is an example of the global mode and distinguished from $f_M=1.00\omega$ for the local Hartmann mode. $f_M=0.70\omega$ is another characteristic frequency of the USGA nozzle besides $f_M=1.00\omega$, which depends on the length of L_1, L_2, and L_3 cooperatively. While, f_M=1.00ω is only decided by L_1, which can be calculated by the quarter-wavelength theory. Analyzing the evolutions of isobaric curves, we find that the pressure wave travels in the nozzle cavity. In Fig. 13, we show the patterns of the pressure wave propagation for the two modes inside the USGA nozzle. It can be seen that, for the Hartmann mode, the pressure waves oscillate mainly between the Hartmann tube and the secondary tube.

While, in the global mode, the waves are generated at the bottom of the Hartmann tube, and after going through the secondary tube, they propagate towards the inlet. Table 2 gives the peak values of f_0, f_{-1}, and f_{-2} when the intaking duct length L_3 increases. It can be clearly seen that f_0 has no change for the variation of L_3, which shows the characteristic of the local oscillation; while the other two are different, and obviously, f_{-1} and f_{-2} are both global and change with L_3.

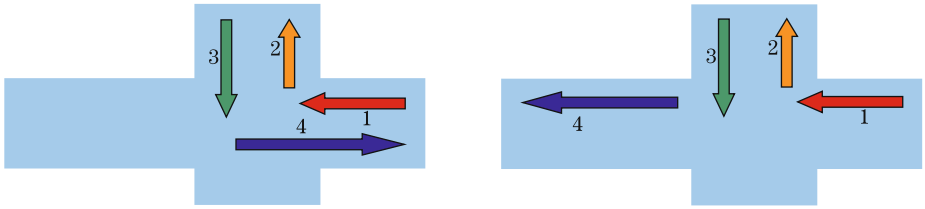

(a) Hartmann mode (b) Global mode

Fig. 13 Two types of propagating routes and their corresponding modes for sound waves generated by oscillation of gas flow in USGA nozzle

Table 2 Comparisons of excited crest values of f_0, f_{-1}, and f_{-2} changing with lengths of inlet duct $L_3 = 5D$, $7D$, and $9D$, respectively

L_3	$5D$	$7D$	$9D$
f_0	1.05ω	1.05ω	1.05ω
f_{-1}	0.70ω	0.55ω	0.45ω
f_{-2}	0.25ω	0.20ω	0.15ω

Suppose that the variation of the sound speed is negligible in the gas flow for the USGA nozzle, and the pressure oscillating frequency $f = 2\pi/\lambda$ is proportional reversely to the distance of the sound propagation in a period, i.e., $f_{-1}/f_0{=}\lambda_0/\lambda_{-1}$. The oscillation in the Hartmann mode begins from the end of the Hartmann tube. Then, it enters into the secondary tube, bounces back from the bottom, and returns to the Hartmann tube to form a closed cycle of the vibration loop (see Fig. 13(a)). While, for the global mode, the wave bouncing back from the bottom of the secondary tube will not enter the Hartmann tube again. Instead, it propagates upstream towards the inlet. Hence, its route is not a closed loop (see Fig. 13(b)). By measuring the length of the path 1-2-3-4 (see Fig. 13) of the sound wave propagation for the Hartmann mode and the global mode, the characteristic frequency for the global mode can be estimated by

$$f_{-1,\text{estimate}} = \frac{2(L_1 + L_2)}{L_1 + 2L_2 + L_3} f_0. \tag{2}$$

In Table 3, the values of f_{-1} and $f_{-1,\text{estimate}}$ are compared when L_3 increases. The results are consistent both in trends and amounts. By observing and analyzing the routes of the pressure wave propagation, adopting the linear acoustic theory, and comparing the numerical results with the estimated analytic results, we find that it is reliable to estimate the frequency of oscillation by the linear acoustic theory for these cases.

Table 3 Comparisons of global mode crest values of f_{-1} with $f_{-1,\text{estimate}}$ for lengths of inlet duct $L_3 = 5D$, $7D$, and $9D$, respectively

L_3	$5D$	$7D$	$9D$
f_{-1}	0.70ω	0.55ω	0.45ω
$f_{-1,\text{estimate}}$	0.72ω	0.61ω	0.52ω

When running the cases without input signals, we find that, even for the same parameters, the numerical results can be different for different initial states. For example, by taking the zero initial velocity fields, the steady state, or the flow field from the adjacent parameters as an initial state, either the Hartmann mode or the global mode can appear unpredictably. Till now, there is no obvious evidence that the USGA nozzle will logically work under the Hartmann mode. However, the simulations show that the USGA nozzle has the tendency of working in the global mode when the outlet/inlet pressure ratio R becomes large, which means that the intaking stream also enters into the circles of oscillation and causes system malfunction. The simulations suggest a feasible alternative to induce the USGA nozzle running in the Hartmann mode by active excitations (see Fig. 12).

To achieve the assumed large amplitude of oscillation, we adopt active excitations on the USGA nozzle. We apply the driving signal of intensity ranging from 0.01 kg/s to 0.15 kg/s with the increment of 0.01 kg/s on the main actuator, record the oscillating mass flow rate at the outlet (for the outlet/inlet pressure ratio $R = 1.6$ and the inlet mass flow rate about 1.1 kg/s), and draw the data in Fig. 14. The three curves are related to $f_{\mathrm{M}} = 0.70\omega$, $f_{\mathrm{M}} = 1.00\omega$, and $f_{\mathrm{M}} = 1.05\omega$, and the starting driving amplitudes for $f_{\mathrm{M}} = 0.70\omega$ and $f_{\mathrm{M}} = 1.05\omega$ are 0.02 kg/s and 0.04 kg/s, respectively, which are the minimal driving signal strengths exciting the oscillations at the frequencies other than the natural one.

When the main actuator and the auxiliary actuator work synchronously, the corresponding fluctuation characteristics are analogous to those of the case of working independently, and only non-obvious substantial disparities are shown. However, the drifting phenomenon of the natural frequency will not happen in the case of $f_0/\omega = 1.00$, while it happens in the case of $f_0^+/\omega = 1.05$ for the solely main actuator and in the case of $f_0^-/\omega = 0.95$ for the auxiliary actuator working alone.

It is also necessary to take the influence of the phase angle of the excitation signal into account. We find that the change of the phase angle will not affect the flow structure in the USGA nozzle with the main actuator and the auxiliary actuator running independently, which is rather different from the situation for the dual actuators. Here, 24 cases are carried out to show a curve plotted in Fig. 15 for the phase angle difference $\Delta\varphi = \varphi_{\mathrm{S}} - \varphi_{\mathrm{M}} \subset [-\pi, \pi]$ with the interval of $\pi/12$.

It shows in Fig. 15 that the phase angle difference plays a big role in the oscillations of the pressure and the mass flow rate, and the crest locates at the value $\Delta\varphi \approx \frac{\pi}{6}$, which represents that the signal of the main actuator will lag behind that of the auxiliary actuator with a phase angle of $\pi/6$ to achieve its maximum oscillating amplitude.

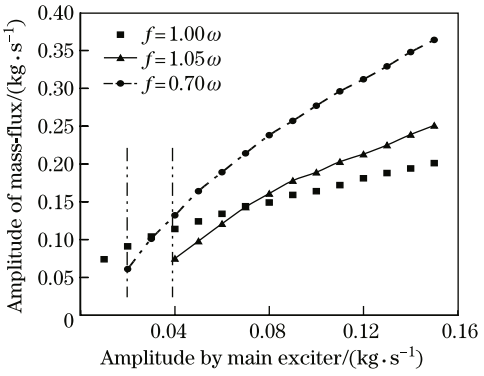

Fig. 14 Variation curves of oscillating amplitude of mass flow rate at USGA nozzle outlet with increasing excitation intensity

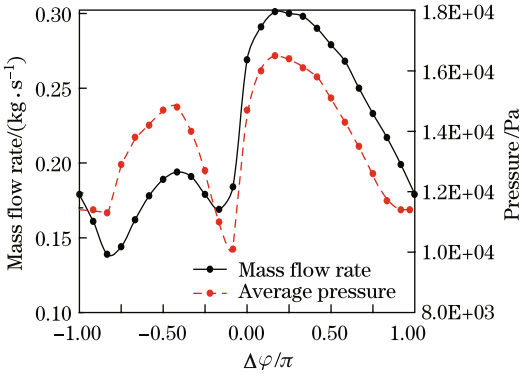

Fig. 15 Fluctuation amplitudes of mass flow rate and pressure with phase angle difference between main and auxiliary actuator signals

5 Conclusions

The main actuator[13–14] and the auxiliary actuator are introduced to construct a double-actuator USGA nozzle. The oscillating characteristics of the gas flow in the USGA nozzle cavity are discussed and analyzed for the outlet/inlet pressure ratio R ranging from 1.000 to 3.000 with or without actuators by numerical simulations.

A convergence-divergence structure analogous to that of the Laval nozzle, namely, the self-adjusting throat, is observed inside the USGA nozzle, which is consistent with the known results[9]. However, the self-adjusting throat has no limitation of the maximum flow rate in the present parameter range. The oscillation of the gas flow starts when R ranges from 1.150 to 1.175, its maximum amplitude reaches at about $R = 2.000$, and the shape of the self-adjusting throat becomes almost invariable after $R = 2.500$.

Besides the main actuator at the end of the Hartmann resonance tube[14], the auxiliary actuator is added to the end of the secondary resonance tube in the same manner. It can be found that the effects of the main actuator and the auxiliary actuator are analogous when they work cooperatively or independently. They are able to (i) enhance the oscillating amplitude of the pressure fluctuation and the mass flow rate vibration at the outlet, and amplify the energy of oscillation greatly; (ii) arouse many different resonant frequencies; (iii) work on two oscillating modes, namely, the Hartmann mode and the global mode.

The drifting phenomenon of the basic frequency occurs when the main actuator[14] or the auxiliary actuator works independently, but does not happen when they work cooperatively. Meanwhile, the difference of the phase angle between the main signal and the auxiliary signal can also cause a dramatic change on the oscillating amplitude, whose peak is found when the main signal lags behind slightly to that of the auxiliary actuator. In addition, the studies show that the secondary tube also plays an important role on gas oscillation, which is confirmed with the cases for which the sizes of the Hartmann tube and the secondary tube are not equal.

References

[1] Hartmann, J. and Trolle, B. A new acoustic generator. *Journal of Scientific Instruments*, **4**, 101–111 (1927)

[2] Raman, G. and Srinivasan, K. The powered resonance tube: from Hartmann's discovery to current active flow control applications. *Progress in Aerospace Sciences*, **45**, 97–123 (2009)

[3] Grant, N. J. Rapid solidification of metallic particulates. *Journal of Metals*, **35**, 20–27 (1983)

[4] Ayres, J. D. and Anderson, I. E. *Method for Generating Fine Sprays of Molten Metal for Spray Coating and Powder Making*, Patent No. 4619845, U. S. A. (1986)

[5] Allimant, A., Planche, M. P., Bailly, Y., Dembinski, L., and Coddet, C. Progress in gas atomization of liquid metals by means of a de Laval nozzle. *Powder Technology*, **190**, 79–83 (2009)

[6] Zhao, W. J., Cao, F. Y., Ning, Z. L., Zhang, G. Q., Li, Z., and Sun, J. F. A computational fluid dynamics (CFD) investigation of the flow field and the primary atomization of the close coupled atomizer. *Computers and Chemical Engineering*, **40**, 58–66 (2012)

[7] Mullis, A. M., McCarthy, I. N., and Cochrane, R. F. High speed imaging of the flow during close-coupled gas atomization: effect of melt delivery nozzle geometry. *Journal of Materials Processing Technology*, **211**, 1471–1477 (2011)

[8] Rai, G., Lavernia, E. J., and Grant, N. J. Powder size and distribution in ultrasonic gas atomization. *Journal of Metals*, **37**(8), 22–26 (1985)

[9] Li, B., Hu, G. H., and Zhou, Z. W. Numerical simulation of flow in Hartmann resonance tube and flow in ultrasonic gas atomizer. *Applied Mathematics and Mechanics* (*English Edition*), **28**(11), 1415–1426 (2007) DOI 10.1007/s10483-007-1101-6

[10] Zhou, Z. W. and Tang, X. D. The effect of the pulsation in gas flow on the stability of melted metal jet. *Fourth International Conference on Spray Forming*, University of Maryland Press, Baltimore, U. S. A. (1999)

[11] Veistinen, M. K., Lavernia, E. J., Baram, J. C., and Grant, N. J. Jet behavior in ultrasonic gas atomization. *The International Journal of Powder Metallurgy*, **25**(2), 89–92 (1989)

[12] Mansour, A., Chigier, N., Shih, T., and Kozarek, R. L. The effects of the Hartman cavity on the performance of the USGA nozzle needed for aluminum spray forming. *Atomization and Sprays*, **1**, 1–24 (1998)

[13] Wang, Z. L. *Actuator Driven Ultra-Sonic Gas Atomization Nozzle*, Patent No. 200810203978, P. R. China (2008)

[14] Zu, H. B. and Wang, Z. L. Resonant behaviors of an ultra-sonic gas atomization nozzle with a zero mass-flux jet actuator. *Journal of Shanghai University* (*English Edition*), **15**(3), 166–172 (2011)

[15] Spalart, P. and Allmaras, S. *A One-Equation Turbulence Model for Aerodynamic Flows*, Technical Report AIAA-92-0439, American Institute of Aeronautics and Astronautics (1992)

[16] Brocher, E., Maresca, A., and Bournay, M. H. Fluid dynamics of the resonance tube. *Journal of Fluid Mechanics*, **43**, 369–384 (1970)

[17] Sreejith, G. J. and Narayanan, S. Studies on conical and cylindrical resonators. *Applied Acoustics*, **69**(12), 1161–1175 (2008)